SIMULATION OPTIMIZATION SYSTEMS
Research Laboratory

ELECTROMAGNETIC OPTIMIZATION EXPLOITING AGGRESSIVE SPACE MAPPING

J.W. Bandler, R.M. Biernacki, S.H. Chen,
R. H. Hemmers and K. Madsen

SOS-95-5-R

February 1995

(Revised July 1995)

McMASTER UNIVERSITY
Hamilton, Canada L8S 4L7
Department of Electrical and Computer Engineering

ELECTROMAGNETIC OPTIMIZATION EXPLOITING AGGRESSIVE SPACE MAPPING

J.W. Bandler, R.M. Biernacki, S.H. Chen,
R. H. Hemmers and K. Madsen

SOS-95-5-R

February 1995

(Revised July 1995)

© J.W. Bandler, R.M. Biernacki, S.H. Chen, R.H. Hemmers and K. Madsen 1995

No part of this document may be copied, translated, transcribed or entered in any form into any machine without written permission. Address enquiries in this regard to Dr. J.W. Bandler. Excerpts may be quoted for scholarly purposes with full acknowledgement of source. This document may not be lent or circulated without this title page and its original cover.

ELECTROMAGNETIC OPTIMIZATION EXPLOITING AGGRESSIVE SPACE MAPPING

John W. Bandler, *Fellow, IEEE*, Radoslaw M. Biernacki, *Senior Member, IEEE*, Shao Hua Chen, *Senior Member, IEEE*, Ronald H. Hemmers, *Student Member, IEEE*, and Kaj Madsen

Abstract

We propose a significantly improved Space Mapping (SM) strategy for electromagnetic (EM) optimization. Instead of waiting for upfront EM analyses at several base points, our new approach aggressively exploits every available EM analysis, producing dramatic results right from the first step. We establish a relationship between the novel SM optimization and the quasi-Newton iteration for solving a system of nonlinear equations. Approximations to the matrix of first-order derivatives are updated by the classic Broyden formula. A high-temperature superconducting microstrip filter design solution emerges after only six EM simulations with sparse frequency sweeps. Furthermore, less CPU effort is required to optimize the filter than is required by one single detailed frequency sweep. We also extend the SM concept to the parameter extraction phase, overcoming severely misaligned responses induced by inadequate empirical models. This novel concept should have a significant impact on parameter extraction of devices.

This work was supported in part by Optimization Systems Associates Inc. and in part by the Natural Sciences and Engineering Research Council of Canada under Grants OGP0007239, OGP0042444 and STR0167080 and through the Micronet Network of Centres of Excellence. Additional support was provided through a Natural Sciences and Engineering Research Council of Canada Graduate Scholarship granted to R.H. Hemmers.

J.W. Bandler, R.M. Biernacki and S.H. Chen are with Optimization Systems Associates Inc., P.O. Box 8083, Dundas, Ontario, Canada L9H 5E7, and with the Simulation Optimization Systems Research Laboratory, Department of Electrical and Computer Engineering, McMaster University, Hamilton, Ontario, Canada L8S 4L7.

R.H. Hemmers is with the Simulation Optimization Systems Research Laboratory, Department of Electrical and Computer Engineering, McMaster University, Hamilton, Ontario, Canada L8S 4L7.

K. Madsen is with the Institute of Mathematical Modeling, Technical University of Denmark, DK-2800 Lyngby, Denmark.

I. INTRODUCTION

In our recent pioneering work [1-4], we introduced the concept of Space Mapping (SM) optimization. The method combines the computational efficiency of empirical engineering circuit models, accumulated and developed over many years, with the acclaimed accuracy of electromagnetic (EM) simulators. This facilitates a highly efficient approach to attacking the demanding EM design process.

In our original formulation of the SM algorithm, an upfront effort was needed in the EM space simply to establish full-rank conditions leading to the initial mapping between the optimization and EM spaces. Since such initial base points are found by simple perturbation around the starting point in the EM space, they are unlikely to produce a substantially better design than the starting point itself. Hence, that approach represents a time-consuming and possibly unproductive effort.

In this paper, we present a significantly improved approach to SM. The method employs a quasi-Newton iteration in conjunction with first-order derivative approximations updated by the classic Broyden formula [5]. From an initial estimate of the EM solution, obtained by an empirical model optimization, we target each costly EM analysis directly at achieving the best EM design. The results are then immediately utilized to improve the approximation. Using this approach, we expect to obtain a progressively improved design after each iteration. This procedure is based on an elegant theoretical formulation and a simple implementation strategy.

One of the key steps in SM is the model parameter identification phase. The SM technique relies on determining pairs of corresponding EM and empirical model points obtained by parameter extraction optimization. Accordingly, we review the appropriate theory and techniques used in traditional parameter extraction. In addition, we describe algorithms based on the idea of Frequency Space Mapping (FSM) [6]. They offer a powerful means of overcoming the problems caused by local minima and model misalignment.

Our new theory and techniques are illustrated through the design of a low-loss narrow-bandwidth high-temperature superconducting (HTS) microstrip filter [3, 4, 6]. We utilize the user-friendly OSA90/hope optimization system with the Empipe interface [7] to the Sonnet *em* field simulator [8].

In Section II, we review the original SM technique. In Section III, we introduce the theory and implementation of our new aggressive SM approach. Section IV reviews traditional parameter extraction optimization and our new FSM algorithms. Sections V-VIII illustrate the design of the HTS microstrip filter. Finally, Section IX contains our conclusions.

II. OVERVIEW OF THE ORIGINAL SPACE MAPPING METHOD

Let the behaviour of a system be described by models in two spaces: the optimization space, denoted by X_{os}, and the EM (or validation) space, denoted by X_{em}. We represent the designable model parameters in these spaces by the vectors x_{os} and x_{em}, respectively. We assume that X_{os} and X_{em} have the same dimensionality, i.e., $x_{os} \in \mathbb{R}^n$ and $x_{em} \in \mathbb{R}^n$, but may not represent the same parameters.

The X_{os}-space model can be comprised of empirical models, or an efficient coarse-grid EM model. Typically, the X_{em}-space model is a fine-grid EM model but, ultimately, can represent actual hardware prototypes if time and resources permit. We assume that the X_{os}-space model responses, denoted by $R_{os}(x_{os})$, are much faster to calculate but less accurate than the X_{em}-space model responses, denoted by $R_{em}(x_{em})$.

In SM optimization, we wish to find a mapping, P, from the X_{em}-space to the X_{os}-space,

$$x_{os} = P(x_{em}) \tag{1}$$

such that

$$R_{os}(P(x_{em})) \approx R_{em}(x_{em}). \tag{2}$$

We assume that such a mapping exists and is one-to-one within some local modeling region encompassing our SM solution. We also assume that, based on (2), for a given x_{em} its image x_{os} in (1) can be found by a suitable parameter extraction procedure, and that this process is unique.

We initially perform optimization entirely in X_{os} to obtain the optimal design x_{os}^*, for instance in the minimax sense, and subsequently use SM to find the mapped solution $\bar{x}_{em}$ in X_{em} as

$$\bar{x}_{em} = P^{-1}(x_{os}^*) \tag{3}$$

once the mapping (1) is established. We designate $\bar{x}_{em}$ as the SM solution instead of x_{em}^* since the mapped solution may only be an approximation to the true optimum in X_{em}.

The mapping is established through an iterative process. In our original work [1-4], we obtained the initial approximation of the mapping, $P^{(0)}$, by performing EM analyses at a preselected set of, at least, m base points in X_{em} around the starting point, where m is the number of fundamental functions [1]. As the first base point we may select the starting point, i.e.,

$$x_{em}^{(1)} = x_{os}^*, \tag{4}$$

assuming x_{em} and x_{os} represent the same physical parameters, and the remaining $m-1$ base points are chosen by perturbation as

$$x_{em}^{(i)} = x_{em}^{(1)} + \Delta x_{em}^{(i-1)}, \quad i = 2, 3, ..., m. \tag{5}$$

This is followed by parameter extraction optimization in X_{os} to obtain the set of corresponding base points $x_{os}^{(i)}$ according to

$$\underset{x_{os}^{(i)}}{\text{minimize}} \ \| R_{os}(x_{os}^{(i)}) - R_{em}(x_{em}^{(i)}) \| \tag{6}$$

for $i = 1, 2, ..., m$, where $\|\cdot\|$ indicates a suitable norm. The additional $m-1$ points apart from $x_{em}^{(1)}$ are required merely to establish full-rank conditions leading to our first approximation to the mapping. Hence, these EM analyses represent an upfront effort before any significant improvement over the starting point can be expected. With the high cost associated with each EM analysis, the additional $m-1$ simulations represent an inefficient component of the algorithm.

At the jth iteration, both sets may be expanded to contain, in general, m_j points which are used to establish the updated mapping $P^{(j)}$. Since the analytical form of P is not available, we use the current approximation $P^{(j)}$ to estimate $\bar{x}_{em}$ in (3), i.e.,

$$x_{em}^{(m_j+1)} = P^{(j)^{-1}}(x_{os}^*). \tag{7}$$

The process continues iteratively until the termination condition

$$\| R_{os}(x_{os}^{*}) - R_{em}(x_{em}^{(m_j+1)}) \| \leq \epsilon \tag{8}$$

is satisfied, where ϵ is a small positive constant. If so, $P^{(j)}$ is our desired P. If not, the set of base points in X_{em} is augmented by $x_{em}^{(m_j+1)}$ and correspondingly, $x_{os}^{(m_j+1)}$ determined by (6) augments the set of base points in X_{os}. Upon termination, we set $\bar{x}_{em} = x_{em}^{(m_j+1)} = P^{(j)^{-1}}(x_{os}^{*})$ as the SM solution.

III. AGGRESSIVE APPROACH TO SPACE MAPPING

Theory

Consider an important property of (8). When approaching the SM solution, the X_{em}-space model response $R_{em}(x_{em}^{(m_j+1)})$ will closely match the optimal X_{os}-space model response $R_{os}(x_{os}^{*})$, within some tolerance ϵ. Hence, after performing an additional parameter extraction optimization in X_{os}, the resulting point $x_{os}^{(m_j+1)} = P(x_{em}^{(m_j+1)})$ approaches the point x_{os}^{*}. Stated more precisely, as $j \rightarrow M$, $x_{os}^{(m_j+1)} \rightarrow x_{os}^{*}$, or

$$\| x_{os}^{(m_j+1)} - x_{os}^{*} \| \leq \eta \quad \text{as} \quad j \rightarrow M \tag{9}$$

where η is a small positive constant and M is the number of iterations needed to converge to an SM solution.

Based on this observation, we can now introduce our new aggressive approach. As in (1), we assume that the vector of X_{os}-space model parameters is a nonlinear vector function, P, of the X_{em}-space model parameters. We define our goal by setting η to 0 in (9). Hence, consider the set of n nonlinear equations

$$f(x_{em}) = 0 \tag{10}$$

of the form

$$f(x_{em}) = P(x_{em}) - x_{os}^{*} \tag{11}$$

where x_{os}^{*} is a given vector (optimal solution in X_{os}).

Let $x_{em}^{(j)}$ be the jth approximation to the solution of (10) and $f^{(j)}$ written for $f(x_{em}^{(j)})$. The next iterate $x_{em}^{(j+1)}$ is found by a quasi-Newton iteration

$$x_{em}^{(j+1)} = x_{em}^{(j)} + h^{(j)} \tag{12}$$

where $h^{(j)}$ solves the linear system

$$B^{(j)} h^{(j)} = -f^{(j)}. \tag{13}$$

$B^{(j)}$ is an approximation to the Jacobian matrix

$$J(x_{em}^{(j)}) = \left[\frac{\partial f^T(x_{em})}{\partial x_{em}} \right]^T \Bigg|_{x_{em} = x_{em}^{(j)}} \tag{14}$$

and is established based on results from all previous iterations. In our implementation, $B^{(1)}$ is set to the identity matrix. The approximation to the Jacobian matrix is updated by the classic Broyden formula [5]

$$B^{(j+1)} = B^{(j)} + \frac{f(x_{em}^{(j)} + h^{(j)}) - f(x_{em}^{(j)}) - B^{(j)} h^{(j)}}{h^{(j)T} h^{(j)}} h^{(j)T}. \tag{15}$$

Incorporating (13) into (15) gives a simplified updating formula

$$B^{(j+1)} = B^{(j)} + \frac{f^{(j+1)} h^{(j)T}}{h^{(j)T} h^{(j)}} \tag{16}$$

where $f^{(j+1)}$ is obtained by evaluating (11) at $x_{em}^{(j+1)}$ using the parameter extraction optimization described in (6).

This new approach is significantly more efficient than our original SM algorithm. The reason for this is that each point $x_{em}^{(j+1)}$ is generated not merely as a base point for establishing the mapping, but also as a step towards the SM solution, which corresponds to solving the nonlinear system of equations (10). Using the new method, we avert from performing time-consuming and possibly unproductive EM analyses at perturbations around the starting point (4). Instead, we begin with a straightforward initial estimate and attempt to improve the EM design in a systematic manner.

Implementation

We now present a straightforward implementation of our new aggressive SM algorithm. First, begin with a point, $x_{os}^* \triangleq arg\ min\{H(x_{os})\}$, representing the optimal design in X_{os} where $H(x_{os})$ is some appropriate objective function. Then, our algorithm proceeds as follows:

Step 0. Initialize $x_{em}^{(1)} = x_{os}^*$, $B^{(1)} = 1$, $f^{(1)} = P(x_{em}^{(1)}) - x_{os}^*$, $j = 1$. Stop if $\| f^{(1)} \| \leq \eta$.

Step 1. Solve $B^{(j)} h^{(j)} = -f^{(j)}$ for $h^{(j)}$.

Step 2. Set $x_{em}^{(j+1)} = x_{em}^{(j)} + h^{(j)}$.

Step 3. Evaluate $P(x_{em}^{(j+1)})$.

Step 4. Compute $f^{(j+1)} = P(x_{em}^{(j+1)}) - x_{os}^*$. If $\| f^{(j+1)} \| \leq \eta$, stop.

Step 5. Update $B^{(j)}$ to $B^{(j+1)}$.

Step 6. Set $j = j + 1$; go to *Step* 1.

Comments

In *Steps* 0 and 3, $P(x_{em})$ is obtained by parameter extraction as described in (6). In *Step* 2, $x_{em}^{(j+1)}$ may be snapped to the closest grid point if the EM simulator uses a fixed-grid meshing scheme. If this is the case, *Step* 5 should employ (15) as the updating formula. The impact of a fixed grid on SM will be investigated in further studies.

IV. MODEL PARAMETER IDENTIFICATION

Review of Traditional Parameter Extraction

One of the key steps of SM involves parameter extraction optimization in order to match responses. For each point x_{em} we need to find a corresponding point x_{os}. Assuming that our response of interest is a function of frequency, define the vector

$$R_{em}(x_{em}) \triangleq [\, R_{em_1}(x_{em}) \;\; R_{em_2}(x_{em}) \;\; \ldots \;\; R_{em_k}(x_{em}) \,]^T \tag{17}$$

where

$$R_{em_i}(x_{em}) \triangleq R_{em}(x_{em}, \omega_i), \quad i = 1, 2, \ldots, k \tag{18}$$

represents the X_{em}-space model response simulated at k frequency points ω_i. For notational brevity, we use $R_{em}(x_{em}, \omega_i)$ to denote a generic response function. In practice, a number of different response functions (such as the scattering parameters $|S_{11}|$ and $|S_{21}|$) may be simultaneously involved in parameter extraction. Also, define the vector

$$\boldsymbol{R}_{os}(\boldsymbol{x}_{os}) \triangleq [\, R_{os_1}(\boldsymbol{x}_{os}) \;\; R_{os_2}(\boldsymbol{x}_{os}) \;\; \ldots \;\; R_{os_k}(\boldsymbol{x}_{os}) \,]^T \tag{19}$$

where

$$R_{os_i}(\boldsymbol{x}_{os}) \triangleq R_{os}(\boldsymbol{x}_{os}, \omega_i), \quad i = 1, 2, \ldots, k \tag{20}$$

represents the X_{os}-space model response.

The extraction problem can be formulated by minimizing a scalar objective function

$$\underset{\boldsymbol{x}_{os}}{\text{minimize}} \;\; H(\boldsymbol{x}_{os}) \tag{21}$$

where H is typically formulated as an ℓ_p norm of the vector of error functions [9]

$$\boldsymbol{e}(\boldsymbol{x}_{os}) \triangleq [\, e_1(\boldsymbol{x}_{os}) \;\; e_2(\boldsymbol{x}_{os}) \;\; \ldots \;\; e_k(\boldsymbol{x}_{os}) \,]^T \tag{22}$$

where the individual errors are defined as

$$e_i(\boldsymbol{x}_{os}) \triangleq w_i [R_{os_i}(\boldsymbol{x}_{os}) - R_{em_i}(\boldsymbol{x}_{em})], \quad i = 1, 2, \ldots, k \tag{23}$$

and w_i are some nonnegative weighting factors. Note, in our parameter extraction formulation, the vector $\boldsymbol{x}_{em}$ and hence $\boldsymbol{R}_{em}(\boldsymbol{x}_{em})$ are fixed while the elements in $\boldsymbol{x}_{os}$ are optimized.

One of our choices for the objective function is the novel Huber norm [10, 11]

$$H(\boldsymbol{x}_{os}) = \sum_{i=1}^{k} \rho_k(e_i(\boldsymbol{x}_{os})) \tag{24}$$

where

$$\rho_k(e_i) \triangleq \begin{cases} e_i^2/2 & \text{if } |e_i| \le k \\ k|e_i| - k^2/2 & \text{if } |e_i| > k \end{cases} \tag{25}$$

which is robust against large errors *and* flexible w.r.t. small variations in the data.

As noted earlier, parameter extraction is an important step in SM. This can be a serious challenge, especially at the starting point if the X_{os}-space model and X_{em}-space model responses

are severely misaligned. By performing a straightforward data-fitting optimization from such a starting point using the traditional approach, the process may be trapped by local minima [6]. To address this issue, we explore significant enhancements to traditional parameter extraction.

A New Approach: Frequency Space Mapping (FSM)

At a given point, typically we will observe a general similarity between the responses $\boldsymbol{R}_{os}$ and $\boldsymbol{R}_{em}$ even if they are severely misaligned. With this in mind, the parameter extraction problem can be better conditioned if we align the responses along the frequency axis first. Specifically, $\boldsymbol{R}_{em}$ is kept fixed while we adjust $\boldsymbol{R}_{os}$ in some appropriate manner. This is accomplished by employing a reference angular frequency $\omega = \omega_{em}$ and a transformed angular frequency ω_{os} related by

$$\omega_{os} = P_{\omega}(\omega). \tag{26}$$

For our purposes, a suitable mapping can be as simple as frequency shift and scaling given by

$$\omega_{os} = \sigma\,\omega + \delta \tag{27}$$

where σ represents a scaling factor and δ an offset.

This brings us to *Phase* 1 of our FSM approach. Here, we need to determine σ_o and δ_o, which effectively aligns $\boldsymbol{R}_{os}$ and $\boldsymbol{R}_{em}$ in the frequency domain. This is done by holding both model parameters $\boldsymbol{x}_{os}$ and $\boldsymbol{x}_{em}$ constant and optimizing only the parameters σ_o and δ_o. This is described by the following optimization:

$$\underset{\sigma_o,\,\delta_o}{\text{minimize}} \;\; \| \boldsymbol{R}_{os}(\boldsymbol{x}_{os}, \sigma_o, \delta_o) - \boldsymbol{R}_{em}(\boldsymbol{x}_{em}) \| \tag{28}$$

where $\|\cdot\|$ is typically the ℓ_2, ℓ_1 or Huber norm. $\boldsymbol{R}_{os}(\boldsymbol{x}_{os}, \sigma_o, \delta_o)$ represents the $\boldsymbol{X}_{os}$-space model response with (20) replaced by

$$R_{os_i}(\boldsymbol{x}_{os}, \sigma_o, \delta_o) \triangleq R_{os}(\boldsymbol{x}_{os}, \sigma_o\omega_i + \delta_o), \quad i = 1, 2, \ldots, k. \tag{29}$$

In *Phase* 2 of our FSM approach, we optimize the $\boldsymbol{X}_{os}$-space model parameters $\boldsymbol{x}_{os}$ such that $\boldsymbol{R}_{os}$ matches $\boldsymbol{R}_{em}$ while again $\boldsymbol{x}_{em}$ remains fixed. In addition, starting from $\sigma = \sigma_o$ and $\delta = \delta_o$ we force σ and δ to obtain the identity mapping ($\sigma = 1$ and $\delta = 0$). We have developed three algorithms to realize this goal: a sequential FSM algorithm (SFSM) and two exact-penalty function

algorithms (EPF), of which one is based on the ℓ_1 norm objective while the other is suitable for minimax optimization.

In the SFSM algorithm, we perform a sequence of optimizations in which the frequency mapping is *gradually* reduced to the identity mapping while x_{os} is optimized at each step. Hence, at the jth iteration of the SFSM algorithm we set both $\sigma^{(j)}$ and $\delta^{(j)}$ and then optimize $x_{os}^{(j)}$ such that R_{os} matches R_{em}. This can be written as

$$\underset{x_{os}^{(j)}}{\text{minimize}} \; \| R_{os}(x_{os}^{(j)}, \sigma^{(j)}, \delta^{(j)}) - R_{em}(x_{em}) \|, \quad j = 0, 1, ..., K \tag{30}$$

where

$$\sigma^{(j)} = 1 + (\sigma_o - 1)\frac{(K - j)}{K} \tag{31}$$

and

$$\delta^{(j)} = \delta_o \frac{(K - j)}{K}. \tag{32}$$

K is set to some integer and determines the number of steps in the sequence. After the full sequence of optimizations, $x_{os}^{(K)}$ is the solution to the parameter extraction problem since $\sigma^{(K)} = 1$ and $\delta^{(K)} = 0$. It should be clear that for larger values of K we increase the probability of success in the parameter extraction problem at the expense of longer optimization time.

In the EPF algorithms, we need to perform only one optimization. The ℓ_1 norm version of the EPF formulation is given by

$$\underset{x_{os}, \sigma, \delta}{\text{minimize}} \; \{ \| R_{os}(x_{os}, \sigma, \delta) - R_{em}(x_{em}) \|_1 + \alpha_1 | \sigma - 1 | + \alpha_2 | \delta | \} \tag{33}$$

where α_1 and α_2 are suitably large positive weighting factors. In the minimax version of the EPF formulation [12], we have

$$\underset{x_{os}, \sigma, \delta}{\text{minimize}} \left\{ \max_{1 \le i \le 4} \left[U(x_{os}, \sigma, \delta), \; U(x_{os}, \sigma, \delta) - \alpha_i g_i \right] \right\} \tag{34}$$

where

$$U(x_{os}, \sigma, \delta) = \| R_{os}(x_{os}, \sigma, \delta) - R_{em}(x_{em}) \|, \tag{35}$$

$$g(\sigma, \delta) = \begin{bmatrix} \sigma - 1 \\ 1 - \sigma \\ \delta \\ -\delta \end{bmatrix} \tag{36}$$

and $\alpha_i > 0$ for $i = 1, 2, 3, 4$. For both EPF formulations, the values of α_i are kept fixed and must be sufficiently large to obtain the identity mapping in (27) and hence the solution to the parameter extraction problem.

While the frequency transformation concept is familiar to microwave engineers, particularly filter designers, here it is defined in a novel way. Our FSM is established through an iterative process and facilitates automated compensation for inadequate modeling. This significantly improves robustness of the parameter extraction phase of the overall SM technique as needed in (6).

V. THE HTS FILTER

We consider the design of a four-pole quarter-wave parallel coupled-line microstrip filter, as illustrated in Fig. 1 [3, 4, 6]. L_1, L_2 and L_3 are the lengths of the parallel coupled-line sections and S_1, S_2 and S_3 are the gaps between the sections. The width $W = 7$ mil is the same for all the sections as well as for the input and output microstrip lines. The input and output line lengths are $L_0 = 50$ mil. The thickness of the lanthanum aluminate substrate used is 20 mil and the dielectric constant is assumed to be 23.425. The design specifications imposed on $|S_{21}|$ are as follows:

$$|S_{21}| \leq 0.05 \quad \text{in the stopband}$$
$$|S_{21}| \geq 0.95 \quad \text{in the passband}$$

where the stopband includes frequencies below 3.967 GHz and above 4.099 GHz and the passband lies in the frequency range [4.008 GHz, 4.058 GHz]. This corresponds to a 1.25% bandwidth. L_1, L_2, L_3, S_1, S_2 and S_3 are considered as design parameters. L_0 and W are kept fixed.

We employ both analytical/empirical models available in OSA90/hope and a fine-grid Sonnet *em* model. The HTS filter empirical model is assembled from fundamental components such as microstrip lines, coupled lines and open stubs. The OSA90/hope empirical model and Sonnet *em* model material and physical parameters are listed in Table I. They are fixed. On a Sun

SPARCstation 10, approximately 1 CPU hour is needed by *em* to simulate the filter at a single frequency for an on-grid point.

VI. EMPIRICAL MODEL DESIGN OF THE HTS FILTER

We started the design of the HTS filter using the OSA90/hope empirical model. The minimax solution is listed in Table II(i). Fig. 2 shows the $|S_{21}|$ and $|S_{11}|$ responses after optimization.

Next, we investigate the robustness of the empirical model nominal solution. The same optimization variables, namely L_1, L_2, L_3, S_1, S_2 and S_3 as in the nominal minimax design are selected. Again, L_0 and W are kept fixed. We perform a number of empirical model minimax optimizations, each starting from a different starting point. We use 50 starting points randomly spread around the minimax solution with a ±1% deviation. Fig. 3(a) plots the $|S_{21}|$ responses for all 50 starting points. The bar chart in Fig. 3(b) depicts the Euclidian distances between the reference minimax solution and the perturbed starting points. Fig. 4 shows the corresponding diagrams after minimax optimizations and clearly illustrates the existence of multiple minimax solutions for the HTS filter. Table II(ii) lists another minimax solution. The responses of the two solutions are nearly identical despite the large numerical deviation in the parameter values.

We perform EM analyses at the two minimax solutions. The *em* results differ significantly from the empirical model responses, as shown in Fig. 5. However, the two *em* analyses exhibit strong similarity. Our aim then, is to use SM to find a solution in the EM space which will substantially reproduce the optimal performance predicted by the empirical model.

VII. ILLUSTRATION OF FSM

A critical step in SM is parameter extraction optimization to match the empirical model response to the EM model response. At the starting point, the empirical and EM model responses may be severely misaligned, as shown in Fig. 6. By performing a straightforward ℓ_1 optimization

from such a starting point, the extraction process can be trapped by a local minimum, as illustrated in Figs. 7 and 8.

We apply our new FSM approach to overcome the difficulties imposed by local minima. First, *Phase* 1 aligns $\boldsymbol{R}_{os}$ and $\boldsymbol{R}_{em}$ along the frequency axis by optimizing the frequency shift and scaling parameters while holding $\boldsymbol{x}_{os}$ and $\boldsymbol{x}_{em}$ fixed, with $\boldsymbol{x}_{os} = \boldsymbol{x}_{em}$. The result is shown in Fig. 9. Next, we initiate *Phase* 2 employing the SFSM algorithm setting $K = 5$ to obtain both the identity mapping and the optimal values of $\boldsymbol{x}_{os}$. Fig. 10 depicts the resulting match.

VIII. AGGRESSIVE SM OPTIMIZATION OF THE HTS FILTER

We perform SM optimization applying our new aggressive SM algorithm with the Broyden update starting from the empirical model minimax solution listed in Table II(i). The SM solution is listed in Table III. This SM result was obtained using only 15 frequency points per EM frequency sweep. The solution emerges after only 6 EM analyses (frequency sweeps). Fig. 11 compares the filter responses of the empirical model optimal design and the ***em*** simulated SM solution.

IX. CONCLUSIONS

We have proposed a new automated Space Mapping approach incorporating the classic Broyden updating formula to aggressively exploit every electromagnetic analysis. We have described and applied our new approach to the electromagnetic design of a high-temperature superconducting microstrip filter. In addition, we have analyzed the robustness of the empirical model nominal solution for this filter indicating the existence of multiple minimax solutions. We have pioneered the application of the Space Mapping concept to the parameter extraction phase by developing new Frequency Space Mapping algorithms in order to overcome poor starting points induced by inadequate empirical models. The application of Frequency Space Mapping significantly improves the robustness of the parameter extraction process which is a key step in Space Mapping optimization.

ACKNOWLEDGEMENT

The authors thank Dr. J.C. Rautio, President of Sonnet Software, Inc., Liverpool, NY, for making *em* available for this work.

REFERENCES

[1] J.W. Bandler, R.M. Biernacki, S.H. Chen, P.A. Grobelny and R.H. Hemmers, "Space mapping technique for electromagnetic optimization," *IEEE Trans. Microwave Theory Tech.*, vol. 42, 1994, pp. 2536-2544.

[2] J.W. Bandler, R.M. Biernacki, S.H. Chen, P.A. Grobelny and R.H. Hemmers, "Exploitation of coarse grid for electromagnetic optimization," *IEEE MTT-S Int. Microwave Symp. Dig.* (San Diego, CA), 1994, pp. 381-384.

[3] J.W. Bandler, R.M. Biernacki, S.H. Chen, W.J. Getsinger, P.A. Grobelny, C. Moskowitz and S.H. Talisa, "Electromagnetic design of high-temperature superconducting microwave filters," *Int. J. Microwave and Millimeter-Wave Computer-Aided Engineering*, vol. 5, 1995, pp. xxx-xxx.

[4] J.W. Bandler, R.M. Biernacki, S.H. Chen, P.A. Grobelny, C. Moskowitz and S.H. Talisa, "Electromagnetic design of high-temperature superconducting microwave filters," *IEEE MTT-S Int. Microwave Symp. Dig.* (San Diego, CA), 1994, pp. 993-996.

[5] C.G. Broyden, "A class of methods for solving nonlinear simultaneous equations," *Math. of Comp.*, vol. 19, 1965, pp. 577-593.

[6] J.W. Bandler, R.M. Biernacki, S.H. Chen, R.H. Hemmers and K. Madsen, "Aggressive space mapping for electromagnetic design," *IEEE MTT-S Int. Microwave Symp. Dig.* (Orlando, FL), 1995, pp. 1455-1458.

[7] *OSA90/hope*™ and *Empipe*™, Optimization Systems Associates Inc., P.O. Box 8083, Dundas, Ontario, Canada L9H 5E7, 1994.

[8] ***em***™ and ***xgeom***™, Sonnet Software, Inc., 135 Old Cove Road, Suite 203, Liverpool, NY 13090-3774, 1994.

[9] J.W. Bandler and S.H. Chen, "Circuit optimization: the state of the art," *IEEE Trans. Microwave Theory Tech.*, vol. 36, 1988, pp. 424-443.

[10] J.W. Bandler, S.H. Chen, R.M. Biernacki, L. Gao, K. Madsen and H. Yu, "Huber optimization of circuits: a robust approach," *IEEE Trans. Microwave Theory Tech.*, vol. 41, 1993, pp. 2279-2287.

[11] J.W. Bandler, S.H. Chen, R.M. Biernacki and K. Madsen, "The Huber concept in device modeling, circuit diagnosis and design centering," *Proc. IEEE Int. Symp. Circuits and Systems* (London, England), 1994, vol. 1, pp. 129-132.

[12] J.W. Bandler and C. Charalambous, "Nonlinear programming using minimax techniques," *J. Optimization Theory and Appl.*, vol. 13, 1974, pp. 607-619.

TABLE I

MATERIAL AND PHYSICAL PARAMETERS
FOR THE OSA90/hope AND *em* MODELS

Model Parameter	OSA90/hope Model Parameter Value	*em* Model Parameter Value
substrate dielectric constant	23.425	23.425
substrate thickness (mil)	19.9516	19.9516
shielding cover height (mil)	∞	250
conducting metal thickness (mil)	1.9685E-2	0
substrate dielectric loss tangent	3.0E-5	3.0E-5
resistivity of metal (Ωm)	0	4.032E-8
surface roughness of metal (mil)	0	-
magnetic loss tangent	-	0
surface reactance (Ω/sq)	-	0
x-grid cell size (mil)	-	1
y-grid cell size (mil)	-	1.75

TABLE II

EMPIRICAL MODEL DESIGN OF THE HTS FILTER

Parameter (mil)	Minimax Solution (i)	Minimax Solution (ii)
L_1	188.33	137.4
L_2	197.98	248
L_3	188.58	138.6
S_1	21.97	17.35
S_2	99.12	120.9
S_3	111.67	75.9

W and L_0 are kept fixed at 7 mil and 50 mil, respectively.

TABLE III

RESULTS OF SM OPTIMIZATION

Parameter (mil)	SM Solution
L_1	181
L_2	201
L_3	180
S_1	19.25
S_2	80.5
S_3	84
Number of EM Analyses	6

All parameter values are rounded to the nearest grid-point. W and L_0 are kept fixed at 7 mil and 50 mil, respectively.

LIST OF FIGURE CAPTIONS

Fig. 1. The structure of the HTS filter [3, 4, 6].

Fig. 2. The OSA90/hope empirical model responses after minimax optimization. (a) $|S_{21}|$ (——) and $|S_{11}|$ (---) for the overall band and (b) the passband details of $|S_{21}|$.

Fig. 3. (a) $|S_{21}|$ of the empirical model at 50 random starting points and (b) the Euclidian distances between the perturbed starting points and the reference minimax solution.

Fig. 4. (a) $|S_{21}|$ of empirical model at the 50 optimized solutions and (b) the Euclidian distances between the optimized solutions and the reference minimax solution.

Fig. 5. A comparison between (a) $|S_{21}|$ and (b) $|S_{11}|$ using the empirical model and ***em*** at the two minimax solutions.

Fig. 6. $\mathrm{Re}\{S_{11}\}$ simulated using the empirical model (——) and ***em*** (---) at the starting point before parameter extraction optimization.

Fig. 7. $\mathrm{Re}\{S_{11}\}$ simulated using the empirical model (——) and ***em*** (---) at the solution of a straightforward ℓ_1 parameter extraction optimization (a local minimum).

Fig. 8. Visualization of the ℓ_1 norm versus two of the model parameters L_2 and L_3; superimposed is the trace of the straightforward ℓ_1 optimization. The optimization converged to a local minimum instead of the true solution represented by the valley near the front of the graph.

Fig. 9. $\mathrm{Re}\{S_{11}\}$ simulated using the empirical model (——) and ***em*** (---) after *Phase* 1 of the FSM algorithm.

Fig. 10. $\mathrm{Re}\{S_{11}\}$ simulated using the empirical model (——) and ***em*** (---) after *Phase* 2 of the FSM algorithm.

Fig. 11. The ***em*** simulated $|S_{21}|$ response of the HTS filter at the solution obtained using the aggressive SM approach (——). The OSA90/hope empirical model solution (---) is shown for comparison. Responses are shown for (a) the overall band and (b) the passband in more detail.

IEEE Trans. Microwave Theory Tech., vol. 43, December 1995

Bandler *et al.* "Electromagnetic optimization exploiting ...", Fig. 1

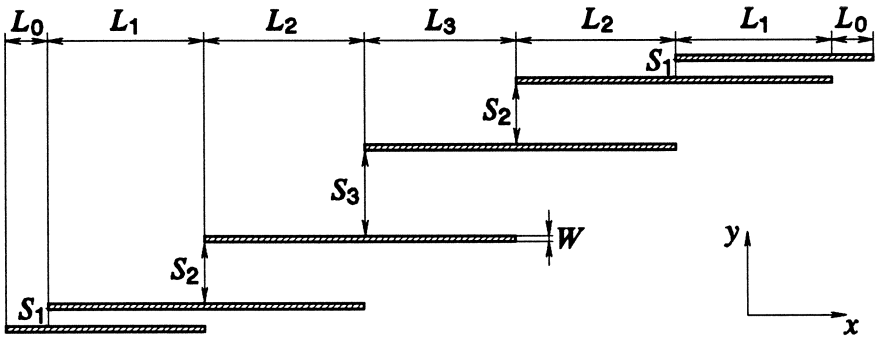

IEEE Trans. Microwave Theory Tech., vol. 43, December 1995

Bandler *et al.* "Electromagnetic optimization exploiting ...", Fig. 2(a)

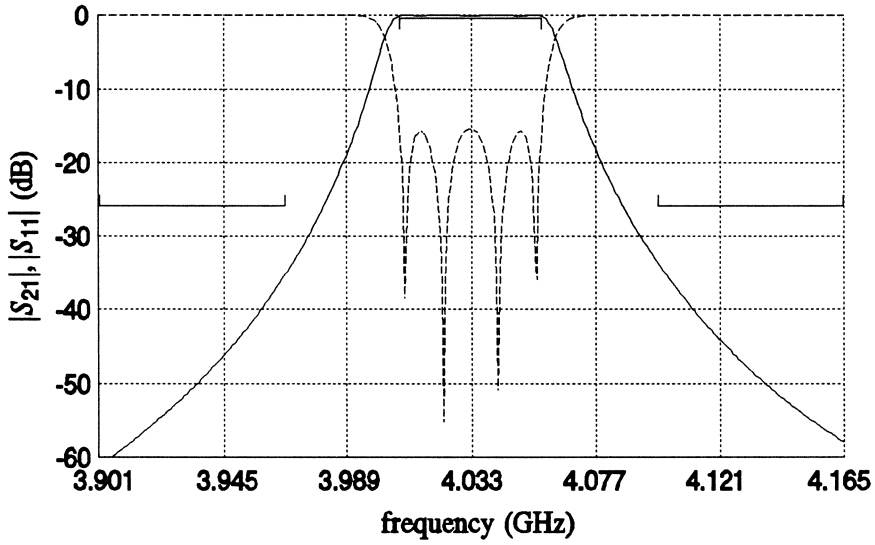

IEEE Trans. Microwave Theory Tech., vol. 43, December 1995

Bandler *et al.* "Electromagnetic optimization exploiting ...", Fig. 2(b)

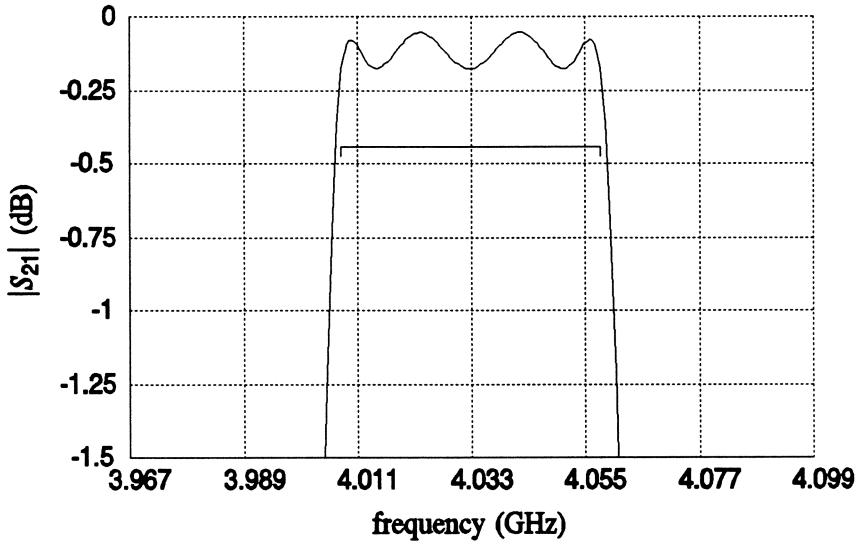

IEEE Trans. Microwave Theory Tech., vol. 43, December 1995

Bandler *et al.* "Electromagnetic optimization exploiting ...", Fig. 3(a)

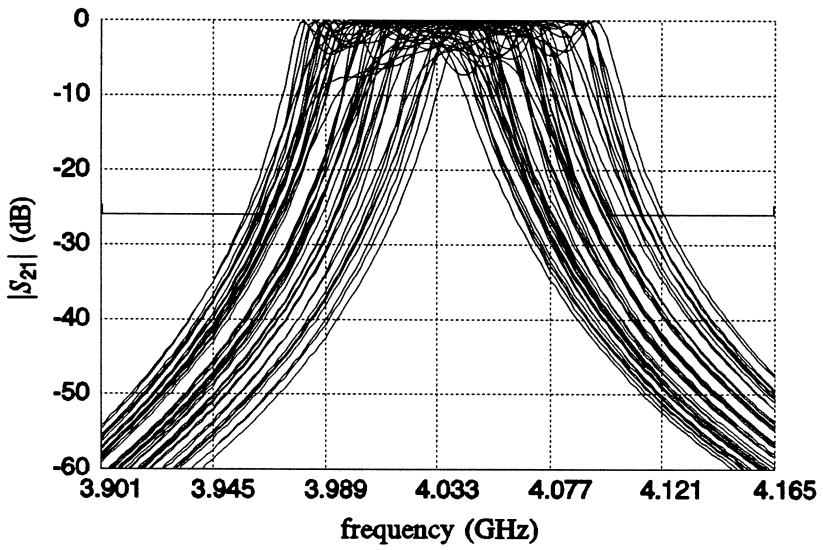

IEEE Trans. Microwave Theory Tech., vol. 43, December 1995

Bandler *et al.* "Electromagnetic optimization exploiting ...", Fig. 3(b)

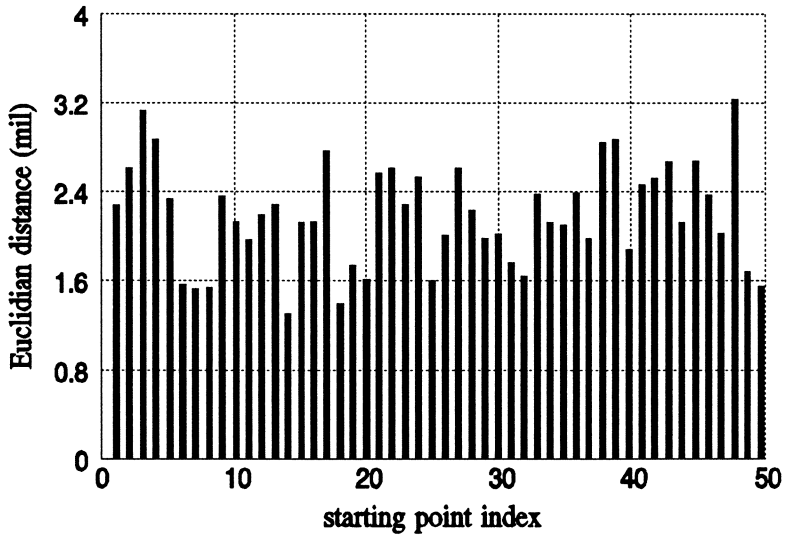

IEEE Trans. Microwave Theory Tech., vol. 43, December 1995

Bandler *et al.* "Electromagnetic optimization exploiting ...", Fig. 4(a)

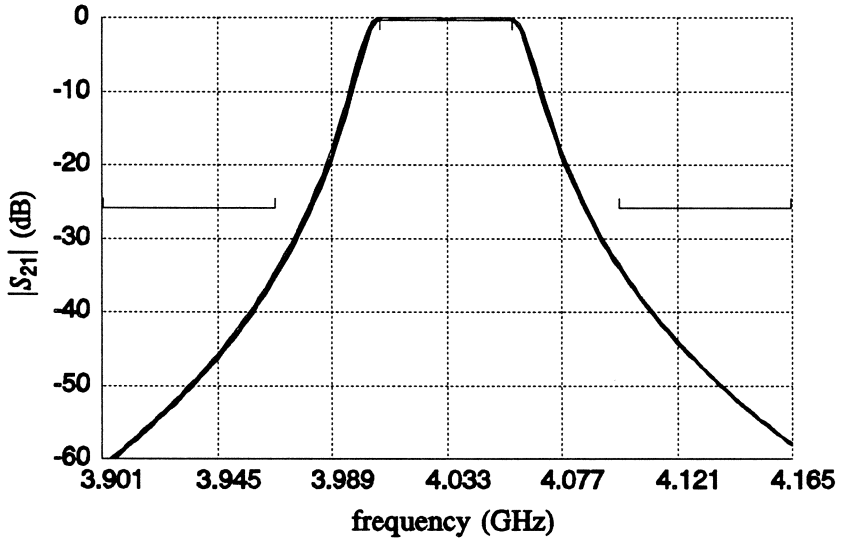

IEEE Trans. Microwave Theory Tech., vol. 43, December 1995

Bandler *et al.* "Electromagnetic optimization exploiting ...", Fig. 4(b)

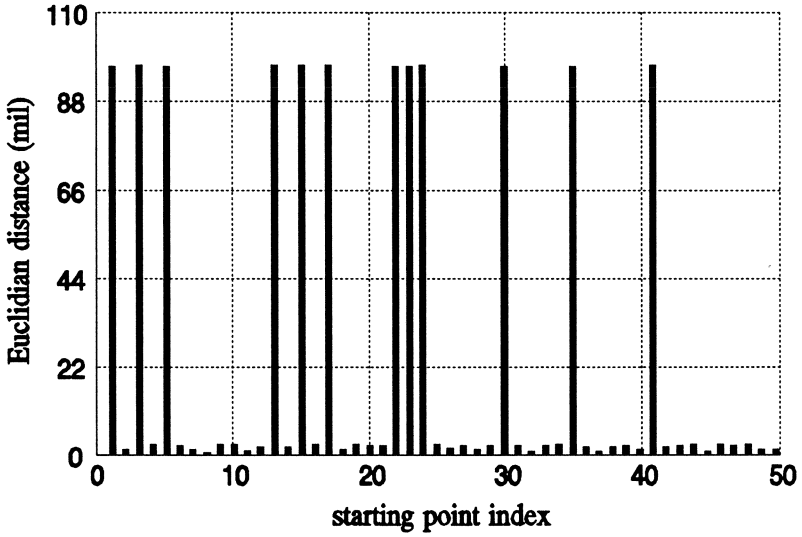

IEEE Trans. Microwave Theory Tech., vol. 43, December 1995

Bandler *et al.* "Electromagnetic optimization exploiting ...", Fig. 5(a)

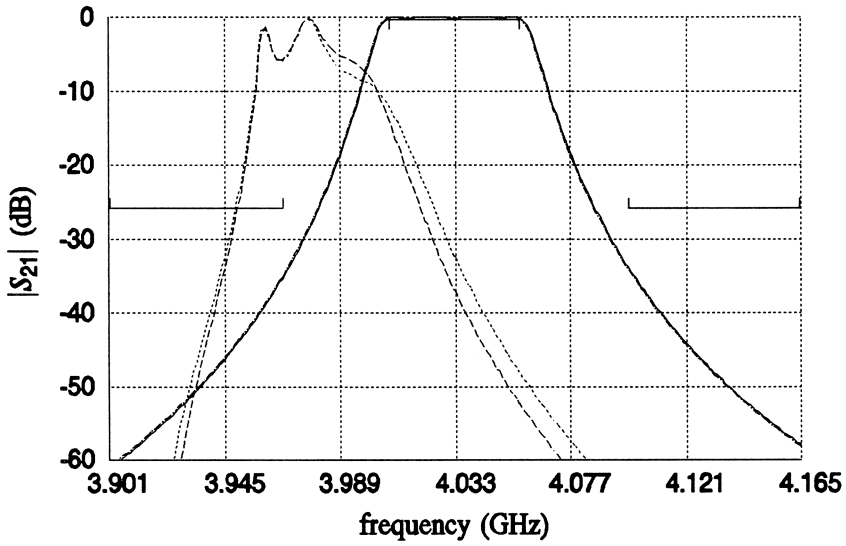

IEEE Trans. Microwave Theory Tech., vol. 43, December 1995

Bandler *et al.* "Electromagnetic optimization exploiting ...", Fig. 5(b)

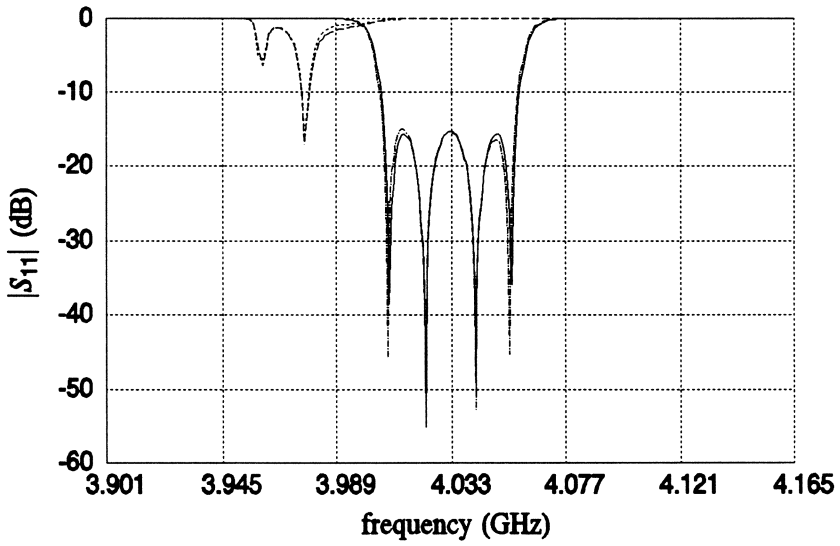

IEEE Trans. Microwave Theory Tech., vol. 43, December 1995

Bandler *et al.* "Electromagnetic optimization exploiting ...", Fig. 6

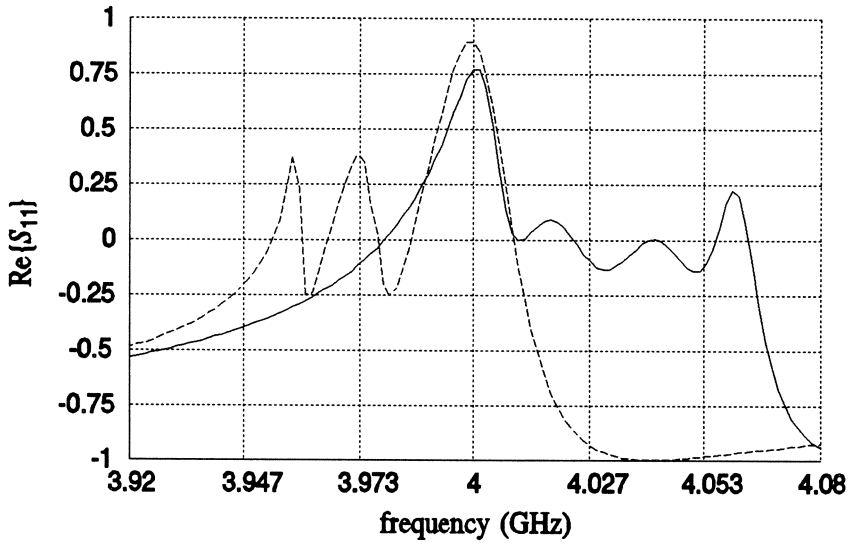

IEEE Trans. Microwave Theory Tech., vol. 43, December 1995

Bandler *et al.* "Electromagnetic optimization exploiting ...", Fig. 7

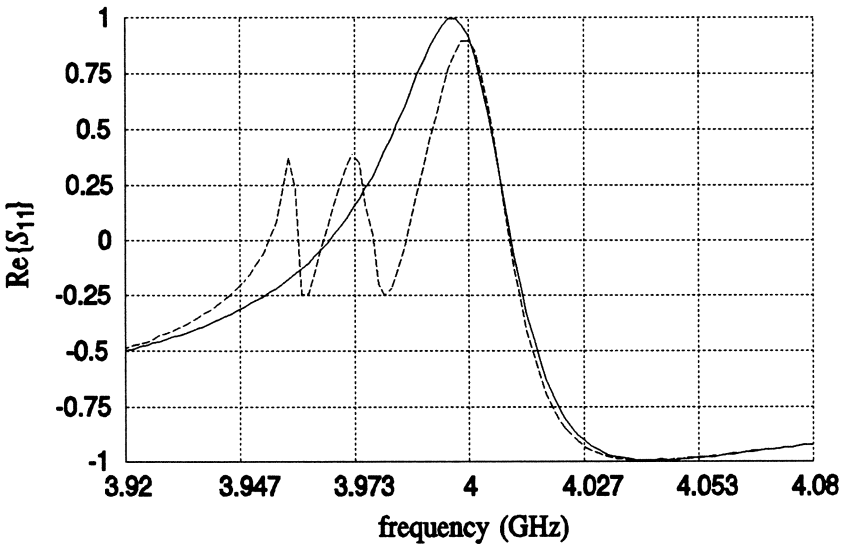

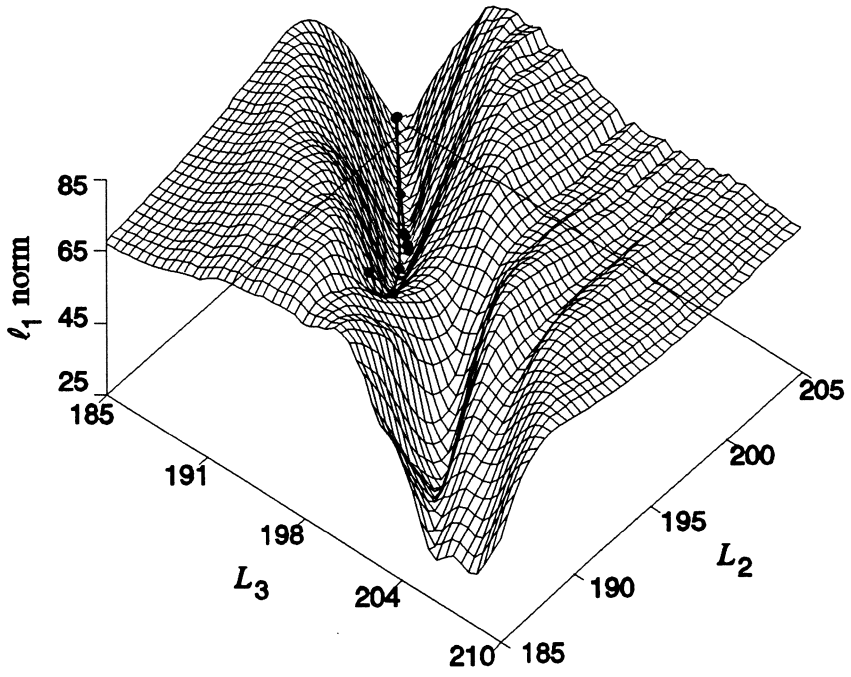
ℓ_1 norm
85
65
45
25
185
191
198
L_3
204
210
185
190
195
200
205
L_2

IEEE Trans. Microwave Theory Tech., vol. 43, December 1995

Bandler *et al.* "Electromagnetic optimization exploiting ...", Fig. 9

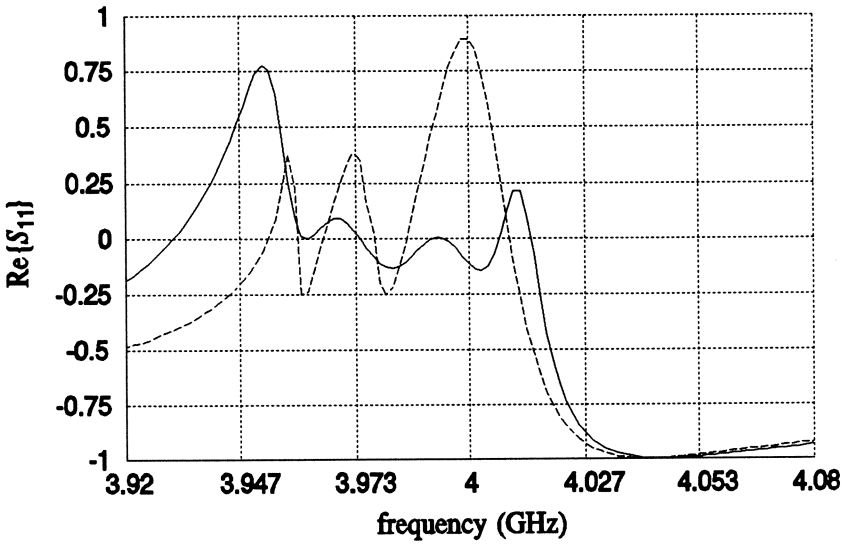

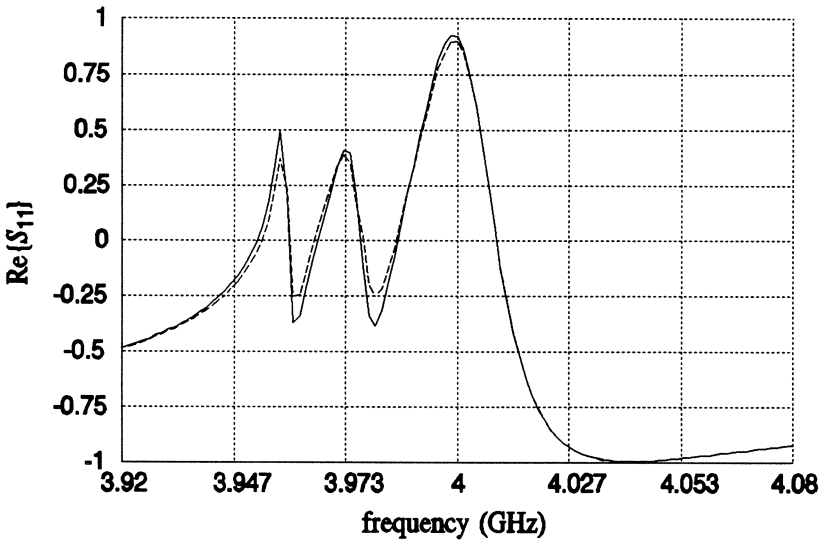
1
0.75
0.5
0.25
0
-0.25
-0.5
-0.75
-1
Re{S11}
3.92
3.947
3.973
4
4.027
4.053
4.08
frequency (GHz)

IEEE Trans. Microwave Theory Tech., vol. 43, December 1995

Bandler *et al.* "Electromagnetic optimization exploiting ...", Fig. 11(a)

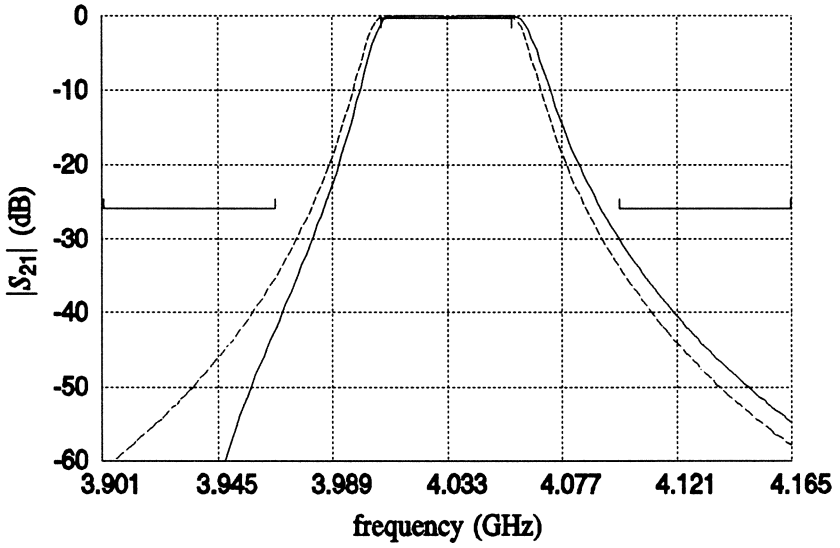

IEEE Trans. Microwave Theory Tech., vol. 43, December 1995

Bandler *et al.* "Electromagnetic optimization exploiting ...", Fig. 11(b)